

Comparing Simultaneous Multi-slice Diffusion Acquisitions

Yogesh Rathi, Borjan Gagoski, Kawin Setsompop, P. Ellen Grant,
and C.-F. Westin

Abstract Diffusion magnetic resonance imaging (dMRI) is an important tool that allows non-invasive investigation of the neural architecture of the brain. Advanced dMRI protocols typically require a large number of measurements for accurately tracing the fiber bundles and estimating the diffusion properties (such as, FA). However, the acquisition time of these sequences is prohibitively large for pediatric as well as patients with certain types of brain disorders (such as, dementia). Thus, fast echo-planar imaging (EPI) acquisition sequences were proposed by the authors in [6, 16], which acquired multiple slices simultaneously to reduce scan time. The scan time in such cases drops proportionately to the number of simultaneous slice acquisitions (which we denote by R). While preliminary results in [6, 16] showed good reproducibility, yet the effect of simultaneous acquisitions on long range fiber connectivity and diffusion measures such as FA, is not known. In this work, we use multi-tensor based fiber connectivity to compare data acquired on two subjects with different acceleration factors ($R = 1, 2, 3$). We investigate and report the reproducibility of fiber bundles and diffusion measures between these scans on two subjects with different spatial resolutions, which is quite useful while designing neuroimaging studies.

Y. Rathi (✉) · C.-F. Westin
Brigham and Women's Hospital, Harvard Medical School, Boston, MA, USA
e-mail: yogesh@bwh.harvard.edu; westin@bwh.harvard.edu

B. Gagoski · P.E. Grant
Boston Children's Hospital, Harvard Medical School, Boston, MA, USA
e-mail: borjan.gagoski@childrens.harvard.edu; Ellen.Grant@childrens.harvard.edu

K. Setsompop
Massachusetts General Hospital, Harvard Medical School, Boston, MA, USA
e-mail: kawin@nmr.mgh.harvard.edu

1 Introduction

High Angular Resolution Diffusion Imaging (HARDI) involves acquiring diffusion information for a single b-value in several gradient directions uniformly spread on a sphere [17]. This protocol allows for resolving the angular structure of the neural fibers, while diffusion spectrum imaging (DSI) proposed by Wedeen et al. [20] provides important information about the radial signal decay, which is sensitive to minor white matter pathology. Both, HARDI and DSI acquisition schemes require several measurements along different gradient directions making them difficult to use in clinical settings. To reduce the scan time, two different yet complimentary approaches have been proposed; (i) *Multi-slice acquisitions*: This approach used the standard MRI hardware to cleverly acquire multiple slices simultaneous, thus reducing the scan time. (ii) *Compressed sensing*: These approaches used the concept of compressed sensing to reconstruct the diffusion signal in q-space from very few measurements. Before these approaches can be used in neuroscience studies, they have to be compared and validated to better quantify their effect on various structures of the brain. In this work, we propose to compare and contrast three simultaneous multi-slice acquisition protocols in terms of their ability to trace fiber tracts and estimate diffusion measures such as, fractional anisotropy (FA), and trace (TR). **Simultaneous multi-slice acquisitions**: Traditional acquisition techniques typically rely on rapid, single-shot two-dimensional (2D) Echo Planar Imaging (EPI) acquisition methods. However, for high-resolution imaging where a large number of slices are needed to cover the brain, a long repetition time (TR) is required. This renders the method inefficient compared with 3D encoding methods. Conventional accelerated 2D parallel imaging approaches [7] can greatly increase the speed of the EPI encoding by eliminating phase encoding steps. Although beneficial for other reasons, this does not translate to a significant reduction in TR or acquisition time, as diffusion sequences contain large, fixed time blocks that cannot be shortened, such as the time for diffusion encoding or the time to a suitable echo time (TE) for T2* contrast.

In comparison, accelerating the data acquisition using the simultaneous acquisition of multiple slices can be very effective as it directly reduces the amount of time needed to acquire a fixed number of slices. For example, if three imaging slices are acquired per shot instead of one, the total acquisition time decreases directly by a factor of 3. When $TR > T1$, then the acquisition can maintain a nearly fully relaxed equilibrium magnetization even for three acceleration. Furthermore, unlike standard parallel imaging techniques, simultaneous multi-slice acquisition methods do not shorten the readout period or omit k-space samples. Therefore, they are not subject to a \sqrt{R} penalty on SNR (where R is the acceleration factor) found in conventional parallel imaging acceleration. Thus, in this work, we use the multi-slice acquisition protocol detailed in [16], which uses both the inplane (acceleration factor of 2) and slice accelerations to simultaneously acquire data from multiple slices. In this case, the repetition time TR is reduced proportionately to the number of multi-slice acquisitions R .

2 Our Contributions

We propose to quantitatively compare three different multi-slice acquisition schemes corresponding to the acceleration factors of $R = \{1, 2, 3\}$ respectively. Existing work in [6, 16] has shown the efficacy of multi-slice acquisitions only at a voxel level and hence its effect on long and short range fiber tracts is not known. Further, a comprehensive analysis of the reproducibility of several diffusion measures, such as, FA and trace has not been done. In this work, we use a multi-tensor unscented Kalman filter (UKF) based tractography algorithm of [2, 10] to obtain full brain connectivity and quantitatively compare fiber bundles from different acquisitions. We also compare the effect of spatial resolution on diffusion measures (FA and trace) and fiber bundle connectivity for the three acceleration factors. Thus, to the best of our knowledge, this is a first such quantitative study on comparing multi-slice acquisitions. Knowing the performance of each type of scan can provide useful information during the design of neuroimaging studies.

3 Methods

Multi-tensor analysis: It is now quite well-known that the single tensor method is inadequate for representing multi-fiber compartments [17]. Consequently, several advanced models have been proposed in the literature to represent the fiber orientation distribution functions (fODF) [1, 4, 11, 12]. However, all of these methods estimate the fODF at each voxel independently and then a separate tractography algorithm is used to trace the fiber tracts. In contrast, the method of [10] does a joint fiber model estimation and tractography, by accounting for the correlation in diffusion of water along the fiber tract while recursively estimating the model parameters. Further, as reported in [2, 13], adding an isotropic “free-water” component to the model can better characterize the signal and produces more accurate fiber tracts. We thus use two-tensors and an isotropic free-water compartment to model our signal S :

$$S(\mathbf{q}_i) = S_0 \left(\frac{w_1}{2} \exp(-b\mathbf{q}_i^T D_1 \mathbf{q}_i) + \frac{w_1}{2} \exp(-b\mathbf{q}_i^T D_2 \mathbf{q}_i) + w_2 e^{-b\mathbf{q}_i^T D_{iso} \mathbf{q}_i} \right) \quad (1)$$

where, $\mathbf{q}_i \in \mathbb{S}^2$ is the gradient direction, $w_1 + w_2 = 1$ and w_i forms the volume fraction of each component, D_1 and D_2 are cylindrical tensors and D_{iso} is an isotropic tensor with fixed diffusivity of $0.003 \text{ mm}^2/\text{s}$ as given in [14]. For a thorough treatment on the UKF based tractography algorithm, please refer to [10] (<http://www.nitrc.org/projects/ukftractography/>).

Metric for comparing fiber bundles: Several metrics have been proposed to compute distances (overlap) between fiber bundles, in the context of fiber bundle registration [5, 19]. In this work, we propose to use the Bhattacharyya metric B

on probability distributions [9] to quantify overlap between fiber bundles, due to its simplicity in computation and interpretation. To compute B , we estimate the probability distribution for each of the spatial co-ordinates (x , y , z) of a fiber bundle using a kernel density estimator [3]. Then, the Bhattacharyya metric in the x -coordinate B_x is given by: $B_x = \int \sqrt{p_1(x)p_2(x)}dx$, where $p_1(x)$, $p_2(x)$ are the pdf's to be compared. To compute the distance between two fiber bundles, we simply take an equally-weighted combination in each co-ordinate:

$$B = \frac{1}{3} \left(\int \sqrt{p_1(x)p_2(x)} dx + \int \sqrt{p_1(y)p_2(y)} dy + \int \sqrt{p_1(z)p_2(z)} dz \right).$$

Note that, if $p_1 = p_2$, then $B_x = \int p_1(x) dx = 1$. Thus, values of B are bounded between 0 and 1. Further, B will be 1 for a perfect match between two fiber bundles and 0 for no overlap at all.

4 Experiments

Data acquisition: We acquired diffusion MRI data on two subjects using the following set of parameters and an in-plane acceleration factor of 2: (1) For subject # 1, we used the following scan parameters: 60 gradient directions at a b-value of 1,000, (echo time) TE = 130 ms, spatial resolution of $2 \times 2 \times 2 = 8 \text{ mm}^3$. Three data sets were acquired for three acceleration factors $R = \{1, 2, 3\}$ with repetition time TR = {10.6, 5.5, 3.7} s respectively. (2) For subject # 2, all parameters were the same, except the spatial resolution, which was $2.5 \times 2.5 \times 2.5 = 15.62 \text{ mm}^3$. A decrease in the spatial resolution from 8 to 15.62 mm^3 increases the SNR by a factor of 2 (proportional to the increase in size of the voxel $\frac{15.62}{8}$). This would allow us to quantify the effect of increased SNR on diffusion measures and tractography. All the diffusion data sets for each subject were aligned to the same co-ordinate system and corrected for motion and eddy current distortion using FLIRT [8]. A T1-weighted image acquired for each subject was parcellated into several gray matter regions (corresponding to the SRI24 atlas) using the CMTK toolkit [15].

To quantify the differences between the acquisitions corresponding to the various acceleration factors, we performed whole brain tractography using the multi-tensor algorithm of [10], with 10 seeds per voxel. All parameters in the tractography algorithm were kept the same for all acquisitions. Fiber bundles connecting 66 different regions of the SRI24 atlas were extracted for each subject. For each fiber bundle, we computed the following error metrics, assuming that the acquisition with $R = 1$ is the ‘‘gold standard’’.

1. Overlap between fiber bundles was computed using B .
2. Percentage difference in FA: $100 \times \frac{(FA_g - FA)}{FA_g}$, where FA_g is the mean FA of the gold standard.

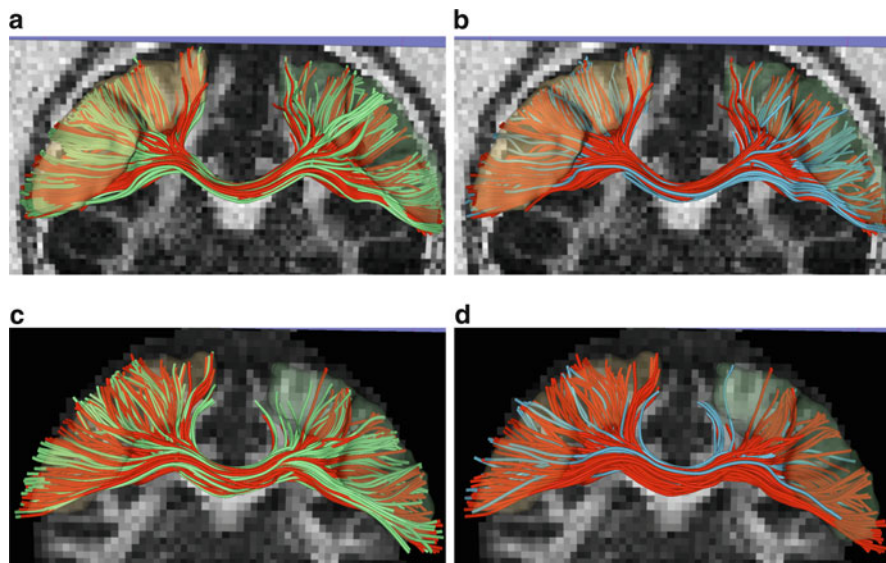


Fig. 1 Qualitative comparison of interhemispheric precentral fibers traced for two subjects and acceleration R of 1 (red), 2 (green), and 3 (blue). Fibers from $R = 2$ data (green) overlap quite well with the standard $R = 1$ (red) protocol for the both subjects. (a) Subject #1, $R = \{1,2\}$. (b) Subject #1, $R = \{1,3\}$. (c) Subject #2, $R = \{1,2\}$. (d) Subject #2, $R = \{1,3\}$

3. Percentage difference in trace (TR): $100 \times \frac{(T_g - T)}{T_g}$, where T_g is the mean trace of the gold standard fiber bundle.

These metrics allow for computing the error in the estimation of the principal diffusion direction(s) and diffusion measures for the various acceleration factors. We should note that, as reported in [16], the SNR decreases with increase in the number of multi-slice acquisitions. Thus, we expect increased error for $R = 3$.

Fiber bundle connectivity: Figure 1 shows the fibers connecting the left and right precentral gray matter regions of the brain for both the subjects. Red fibers indicate “gold standard” with $R = 1$, while green and blue indicate fibers traced with $R = 2$ and $R = 3$ respectively. Since the number of voxels in subject #2 is less (due to lower spatial resolution), the overall number of fibers are fewer compared to subject #1.

Fiber bundle overlap: Figure 2 shows a fiber connectivity graph color coded with the fiber bundle overlap measure B between the gold standard $R = 1$ and the fast acquisitions with $R = 2, 3$ for both the subjects. We observe that in both the cases, there is a significant overlap (around 0.9) for the case of $R = 2$, while it decreases in several fiber bundles for $R = 3$. Specifically, at higher spatial resolution (subject #1), the noise for $R = 3$ acceleration significantly affects the tractography algorithm causing reduced overlap compared to a similar acquisition for subject #2 (with lower

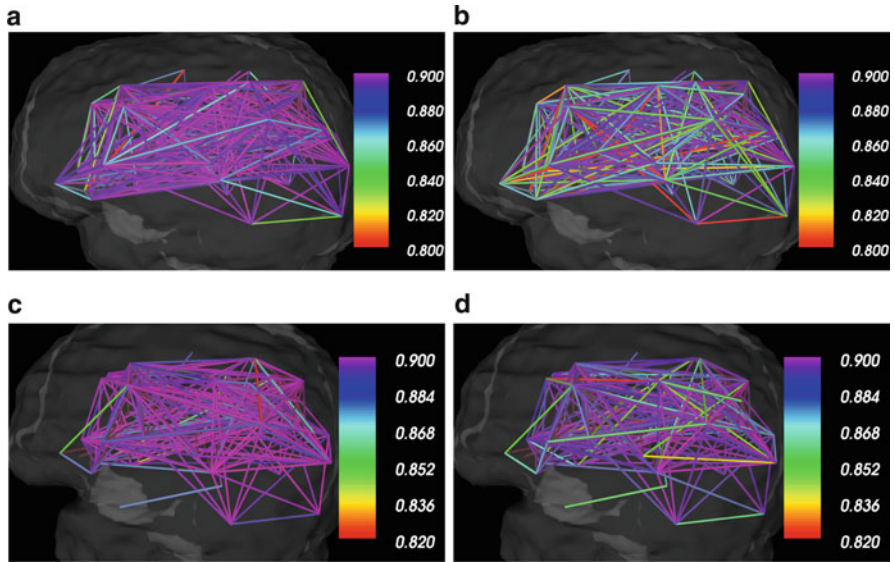


Fig. 2 Fiber bundle connectivity graph color coded with overlap measure B for both the subjects. In general, overlap is close to 0.9 for both subjects for $R = 2$. Increased SNR due to bigger voxel size in subject #2 produces better overlap for $R = 3$. (a) Subject #1, overlap B for $R = \{1,2\}$. (b) Subject #1, overlap B for $R = \{1,3\}$. (c) Subject #2, overlap B for $R = \{1,2\}$. (d) Subject #2, overlap B for $R = \{1,3\}$

spatial resolution). However, in general, for both the subjects, the overlap always exceeds $B = 0.8$ for all fiber bundles.

Reproducibility in FA: For each fiber bundle, we also computed the percentage difference in FA for the $R = \{2, 3\}$ accelerations factors. For the case of $R = 2$, most fiber bundles showed less than 8% difference in estimation of FA (with a few exceptions). This is in line with other single tensor based studies that have reported an average variability of about 5% in white matter and 10–15% in gray matter between scans of the same subject on the same scanner [18]. In our case, since the tractography algorithm traces tracts well into the gray matter, the average difference in FA (of white matter) was slightly higher as given in Table 1. Further, as seen in Figs. 3 and 4, the accelerated acquisitions result in an overall decrease in estimation of FA and trace.

Reproducibility in Trace (TR): As seen in Fig. 4 (and Table 1), trace is less affected with the multi-slice acquisitions compared to FA. However, an overall decrease in trace is noticed for all accelerated acquisitions, albeit within the range of variability seen in standard acquisitions.

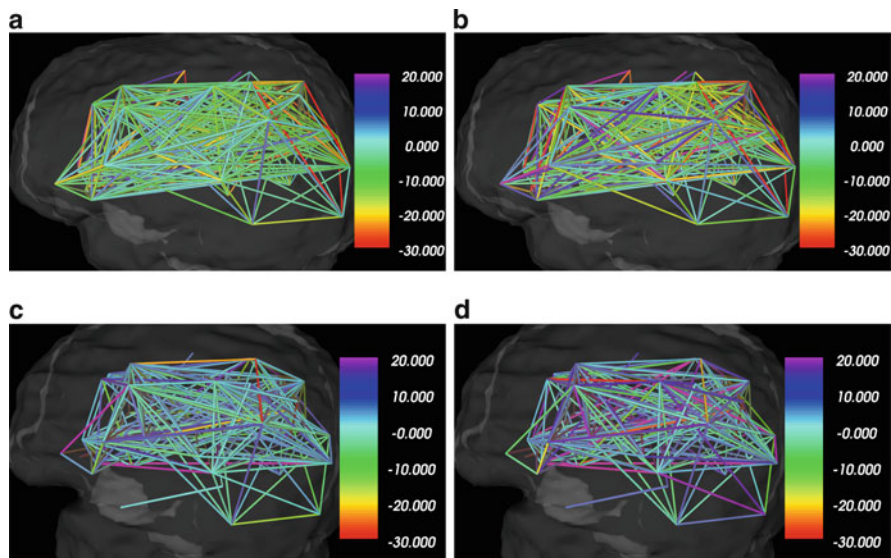


Fig. 3 Connectivity graph is color coded with percentage difference in FA for fast acquisitions. $\pm 6\%$ difference is observed for most fiber bundles for $R = 2$ acquisition (both subjects), whereas the difference is quite high for $R = 3$ in both subjects. (a) Subj. #1, % FA difference in $R = \{1,2\}$. (b) Subj. #1, % FA difference in $R = \{1,3\}$. (c) Subj. #2, % FA difference in $R = \{1,2\}$. (d) Subj. #2, % FA difference in $R = \{1,3\}$

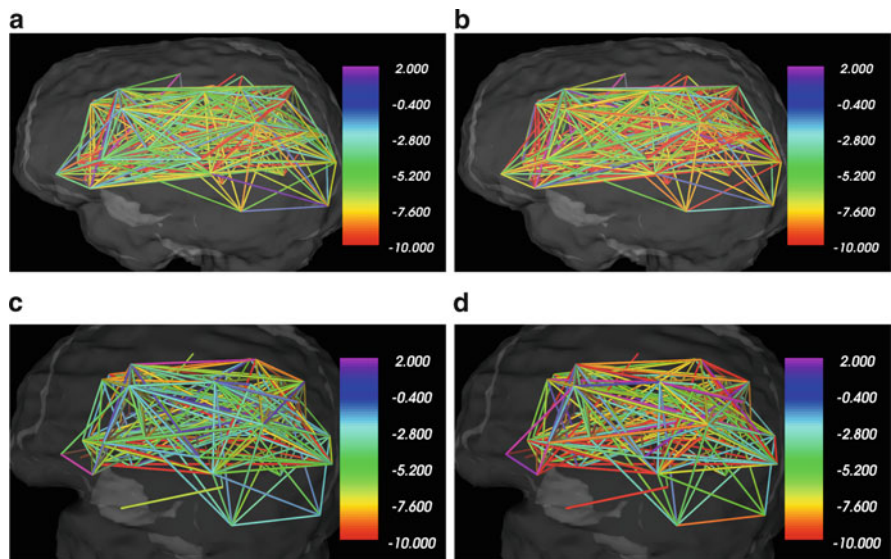


Fig. 4 Connectivity graph is color coded with percentage difference in trace (TR) observed between the acquisitions. $\pm 6\%$ is observed for most fiber bundles for $R = 2$ acquisition (both subjects), whereas the difference is quite high for $R = 3$. (a) Subj. #1, % TR difference in $R = \{1, 2\}$. (b) Subj. #1, % TR difference in $R = \{1, 3\}$. (c) Subj. #2, % TR difference in $R = \{1, 2\}$. (d) Subj. #2, % TR difference in $R = \{1, 3\}$

Table 1 Average percentage difference in estimation of whole brain FA and trace

–	FA		TR	
	$R = 2$	$R = 3$	$R = 2$	$R = 3$
Subject # 1 (%)	7.70	9.63	6.03	8.32
Subject # 2 (%)	4.96	7.39	4.55	6.10

5 Conclusion

In this work, we compared simultaneous multi-slice acquisitions of diffusion MRI on two subjects with acceleration factors of $R = \{1, 2, 3\}$. We used a multi-tensor tractography algorithm to trace several fiber bundles of the brain and investigated the fiber bundle overlap and reproducibility of diffusion measures such as FA and trace compared to the standard acquisition of $R = 1$. Further, we investigated the effect of spatial resolution (2 mm vs 2.5 mm isotropic) on such acquisitions. While preliminary in nature, we can draw the following inferences from the results obtained: (i) Fiber bundles obtained from the $R = 2$ acceleration factor show a very good overlap (close to 0.9) with the standard acquisition for both spatial resolutions. For $R = 3$, the overlap is lower, yet greater than 0.8 in all cases. Thus, the orientation of white matter fibers is not significantly affected in accelerated scans, as also reported in [16]. (ii) For $R = 2$, the average variation in FA and trace is similar to that reported in standard ($R = 1$) test-retest studies [18]. However, there are a few fiber bundles that show a significantly higher difference in FA. This could potentially be due to the increased noise in accelerated scans affecting the tractography algorithm. (iii) For $R = 3$, several fiber bundles showed significant deviation in diffusion measures compared to the gold standard. (iv) Since the lower resolution scan of subject # 2 had better SNR, it was reflected in lower variance in the estimated FA and trace (see Table 1). However, due to significant partial voluming, we observed fewer or no connections between a few gray matter regions for this subject (even in the “gold standard” scan). Thus, overall, lower spatial resolution while increasing the SNR, performed at sub-par levels in terms of finding connections between regions. Overall, an accelerated acquisition with $R = 2$ could safely be used in neuroimaging studies. We should however note that, this work is quite preliminary and needs to be augmented with a comprehensive comparison on several subjects, which is part of our future work.

Acknowledgements This work has been supported by NIH grants: R01MH097979 (YR), R01MH074794 (CFW), P41RR013218, P41EB015902 and Swedish VR grant 2012–3682(CFW).

References

1. Barmpoutis, A., Vemuri, B., Forder, J.: Fast displacement probability profile approximation from hardi using 4th-order tensors. In: ISBI, Paris, pp. 911–914 (2008)
2. Baumgartner, C., Michailovich, O., Levitt, J., Pasternak, O., Bouix, S., Westin, C., Rathi, Y.: A unified tractography framework for comparing diffusion models on clinical scans. In: CDMRI Workshop – MICCAI, Nice (2012)

3. Bowman, A.W., Azzalini, A.: *Applied Smoothing Techniques for Data Analysis*. Oxford University Press, New York (1997)
4. Descoteaux, M., Angelino, E., Fitzgibbons, S., Deriche, R.: Regularized, fast, and robust analytical Q-ball imaging. *Magn. Reson. Med.* **58**, 497–510 (2007)
5. Durrleman, S., Fillard, P., Pennec, X., Trounev, A., Ayache, N.: Registration, atlas estimation and variability analysis of white matter fiber bundles modeled as currents. *NeuroImage* **55**(3), 1073–1090 (2011)
6. Feinberg, D., Moeller, S., Smith, S., Auerbach, E., Ramanna, S., Glasser, M., Miller, K., Ugurbil, K., Yacoub, E.: Multiplexed echo planar imaging for sub-second whole brain fMRI and fast diffusion imaging. *PLoS One* **5**(12), e15710 (2010)
7. Griswold, M.A., Jakob, P.M., Heidemann, R.M., Nittka, M., Jellus, V., Wang, J., Kiefer, B., Haase, A.: Generalized autocalibrating partially parallel acquisitions (grappa). *Magn. Reson. Med.* **47**(6), 1202–1210 (2002)
8. Jenkinson, M., Smith, S., et al.: A global optimisation method for robust affine registration of brain images. *Med. Image Anal.* **5**(2), 143–156 (2001)
9. Kailath, T.: The divergence and bhattacharyya distance measures in signal selection. *IEEE Trans. Commun. Technol.* **15**(1), 52–60 (1967)
10. Malcolm, J.G., Shenton, M.E., Rathi, Y.: Filtered multi-tensor tractography. *IEEE Trans. Med. Imaging* **29**, 1664–1675 (2010). doi:10.1109/TMI.2010.2048121
11. Merlet, S., Caruyer, E., Ghosh, A., Deriche, R., et al.: Parametric dictionary learning in diffusion MRI. In: *HARDI Reconstruction Workshop-ISBI-International Symposium on Biomedical Imaging*, Barcelona (2012)
12. Michailovich, O., Rathi, Y., Dolui, S.: Spatially regularized compressed sensing for high angular resolution diffusion imaging. *Med. Imaging, IEEE Trans.* **30**(5), 1100–1115 (2011)
13. Panagiotaki, E., Schneider, T., Siow, B., Hall, M.G., Lythgoe, M.F., Alexander, D.C.: Compartment models of the diffusion mr signal in brain white matter: a taxonomy and comparison. *NeuroImage* **59**(3), 2241–2254 (2012)
14. Pasternak, O., Sochen, N., Gur, Y., Intrator, N., Assaf, Y.: Free water elimination and mapping from diffusion MRI. *MRM* **62**(3), 717–730 (2009)
15. Rohlfing, T., Zahr, N.M., Sullivan, E.V., Pfefferbaum, A.: The SRI24 multichannel atlas of normal adult human brain structure. *HBM* **31**(5), 798–819 (2009)
16. Setsompop, K., Gagoski, B.A., Polimeni, J.R., Witzel, T., Wedeen, V.J., Wald, L.L.: Blipped-controlled aliasing in parallel imaging for simultaneous multislice echo planar imaging with reduced g-factor penalty. *Magn. Reson. Med.* **67**(5), 1210–1224 (2011)
17. Tuch, D., Reese, T., Wiegell, M., Wedeen, V.: Diffusion MRI of complex neural architecture. *Neuron* **40**, 885–895 (2003)
18. Vollmar, C., O’Muircheartaigh, J., Barker, G.J., Symms, M.R., Thompson, P., Kumari, V., Duncan, J.S., Richardson, M.P., Koeppe, M.J.: Identical, but not the same: intra-site and inter-site reproducibility of fractional anisotropy measures on two 3.0 t scanners. *Neuroimage* **51**(4), 1384–1394 (2010)
19. Wassermann, D., Bloy, L., Kanterakis, E., Verma, R., Deriche, R.: Unsupervised white matter fiber clustering and tract probability map generation: applications of a gaussian process for white matter fibers. *NeuroImage* **51**(1), 228 (2010)
20. Wedeen, V., Hagmann, P., Tseng, W., Reese, T., Weisskoff, R.: Mapping complex tissue architecture with diffusion spectrum magnetic resonance imaging. *Magn. Reson. Med.* **54**(6), 1377–1386 (2005)